Journal of Computational and Nonlinear Dynamics. Received December 06, 2017;
Accepted manuscript posted July 16, 2018. doi:10.1115/1.4040870

Anti-Jerk Dynamic Modeling and Parameter Identification of an Electric Vehicle Based on Road Tests

Mohit Batra, Postdoctoral Fellow
Systems Design Engineering
University of Waterloo
Ontario, Canada
Email: m2batra@uwaterloo.ca

John McPhee, Professor
Systems Design Engineering
University of Waterloo
Ontario, Canada
Email: mcphee@uwaterloo.ca

Nasser L. Azad, Associate Professor
Systems Design Engineering
University of Waterloo
Ontario, Canada
Email: nlashgarianazad@uwaterloo.ca

ABSTRACT

Model-based design facilitates quick development of vehicle controllers early in the development cycle. The goal is to develop simple, accurate, and computationally efficient physics based models that are capable of real-time simulation. We present models that serve the purpose of both plant and anti-jerk control design of electric vehicles. In this research, we propose a procedure for quick identification of longitudinal dynamic parameters for a high-fidelity plant and control-oriented model of an electric vehicle through road tests. Experimental data was gathered on our test vehicle, a Toyota Rav4EV, using an integrated measurement system to collect data from multiple sensors. A MATLAB/Simulink non-linear least square parameter estimator with a trust-reflective algorithm was used to identify the vehicle parameters. The models have been validated against experimental data.

1 Introduction

Advances in vehicle control systems and reduced development time have necessitated quick and accurate development of vehicle models. A significant savings in development time are possible, if an accurate model is available. The accuracy

of these models depends on the parameters used, which are identified through parameter identification techniques. Further, the development of improved controllers is impossible without parameter identification on the complete vehicle subsystems.

In general, vehicle parameters are estimated using commercial testbeds [1]. Standard test procedures like null point method, weight balance method and pendulum tests [2], which have been developed for measuring center of gravity of a vehicle, entail the use of a dedicated test facility [3]. The standard test procedure for measuring tire parameters as per ASTM J199801 involves tire testing on a belt-type flat surface machine. For example, tire testing extends into several days and requires 15 to 20 new tires to gather accurate data. The tire behaviour during laboratory tests is not as good as on-road tests [4] due to differences in texture of road surface, ambient temperature, road crown and road alignment. Vehicle manufacturers are researching methods [5] to get test bench test data as close as possible to that obtained during on-road tests. Moreover, standardized test methods are expensive [6] and time-consuming.

This paper explains how on-road performance measurement systems and numerical parameter identification methods can substantially reduce the need for standardized testing on test beds for vehicles. Experimental data was gathered on our test vehicle, Toyota Rav4EV, using an integrated measurement system designed to simultaneously collect data by integrating an array of sensors including a Vehicle Measurement System (VMS), Global Position Sensor (GPS), Inertial Measurement Unit (IMU), and the vehicle Controller Area Network (CAN).

The MapleSim software has been chosen in this research to build models capable of real-time simulation due to its capability for optimized code-generation. Accordingly, an 18 degree of freedom (DOF) high-fidelity longitudinal dynamics plant model has been developed for the Rav4EV.

Since Electric Vehicles (EVs) are susceptible to torsional oscillations, which are mainly influenced by flexibility in the halfshaft and wheel slip, a reduced control-oriented model capable of anti-jerk control of EVs is required. Most anti-jerk control-oriented models for vehicles are based on damping halfshaft torsion only [7–9]. These models assume the tire as a rigid body, where tire-road friction effects, which are responsible for driveline oscillations in EVs especially during tip-in and tip-out maneuvers are excluded. We have included a more realistic anti-jerk model, which includes tire-friction effects in addition to halfshaft torsion. We have used the linear-tire as well as the Pacejka 2002-tire to model the road friction.

A two-stage parameter optimization procedure is proposed to identify the parameters of the high-fidelity plant model and control-oriented model. First, simple mathematical sub-system models have been considered to identify the individual parameters for the two models. The parameters identified using this approach were then optimized together using the plant model and the control-oriented model to obtain the final set of parameters. A MATLAB/Simulink based non-linear least square parameter estimator with a trust region reflective algorithm [10] was used to identify the parameters by minimizing the difference between experimental and simulated data.

Key contributions presented in this paper are: (a) Use of an integrated measurement system for parameter identification based on road tests thereby eliminating the need for standardized tests (b) Identification of all parameters for the longitudinal dynamics and control-oriented models from simpler on-road tests (c) Develop real-time implementable anti-jerk plant and control-oriented models for EVs, which include wheel-slip effects in addition to halfshaft torque.

A description of the experimental measurement system is presented in Section 2 and experimental tests conducted in

Section 3. The procedure proposed for parameter identification is discussed in Section 4. The MapleSim longitudinal dynamics model is presented in Section 5 and control-oriented models in Section 6. The results of experimental validation of the models are presented in Section 7.

2 Experimental Measurement System

Experimental data was recorded by integrating an array of sensors that includes a Vehicle Measurement System (VMS), Global Position Sensor (GPS), Inertial Measurement Unit (IMU), and the vehicle Controller Area Network (CAN). A CAN integration device from 'Vector Informatik GmbH' was used to integrate the various signals. The system architecture for integrating the signals from the various devices is shown in Fig. 1. A brief description of the various sensors is as follows:

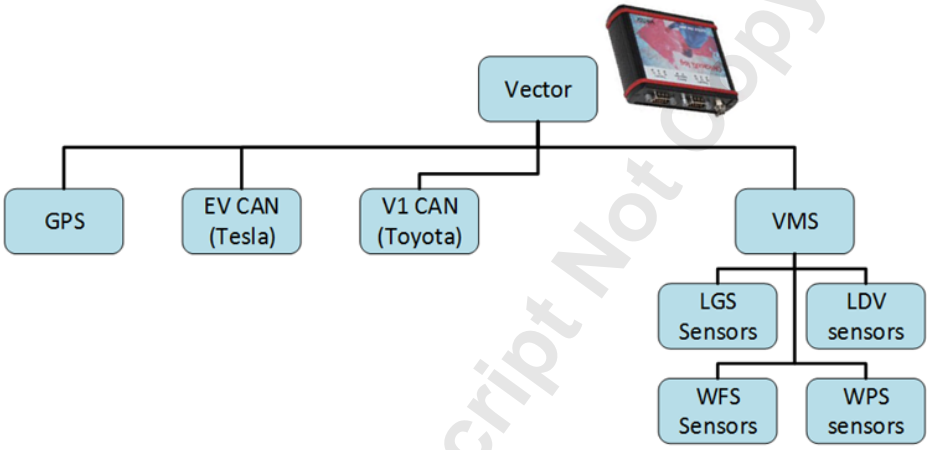

Fig. 1: Integration of sensors through Vector CAN box

Vehicle Measurement System (VMS). The VMS manufactured by '*AnD Technologies*' consists of a sensor set mounted on each of the four wheels to record signals during on-road testing. Each VMS sensor set mounted on a wheel consists of the following five sensors:

(a) **Wheel Force Sensor (WFS) and Rotary encoder.** The WFS is a strain gauge based sensor mounted on a custom wheel hub to record forces (F_x, F_y, F_z) and moments (M_x, M_y, M_z) on the wheel. The wheel hub also houses a rotary encoder to measure the angular speed of wheel.

(b) **Wheel Position Sensor (WPS).** The WPS consists of five digital encoders mounted on a frame that connects the wheel to the chassis. The sensor measures the relative displacement and rotation of the wheel about the longitudinal, lateral and vertical axis with respect to the vehicle body. A picture of WFS and WPS sensors installed on the vehicle is shown in Fig. 2.

(c) **Laser Ground Sensors (LGS) and Laser Doppler Velocimeters (LDV).** The LGS and LDV sensors are mounted together as a single unit on the wheel hub as shown in Fig. 3.

(a) WFS sensor

(b) WPS sensor

Fig. 2: WFS and WPS sensors mounted on wheel hub

Fig. 3: LGS and LDV sensor set mounted on wheel hub

The LGS comprises three laser sensors that compute the dynamic radius of the wheel, or distance of the wheel center from the ground. The two LDV sensors are used to compute the ground speed of the tire in longitudinal and lateral directions. In addition to measuring the dynamic radius, the LGS and LDV sensors are interfaced to compute the slip angle, camber angle, pitch angle and roll angle of the tire by processing the measured data from the sensor set.

Global Position Sensor (GPS) and Inertial Measurement Unit (IMU). An integrated GPS and IMU sensor unit manufactured by Racelogic was used to measure the pitch, roll and yaw rate of the vehicle using rate gyroscopes, and longitudinal, lateral and vertical accelerations using accelerometers. The GPS and IMU sensors are co-located on the roof of the car with the help of a magnetic base as shown in Fig. 4.

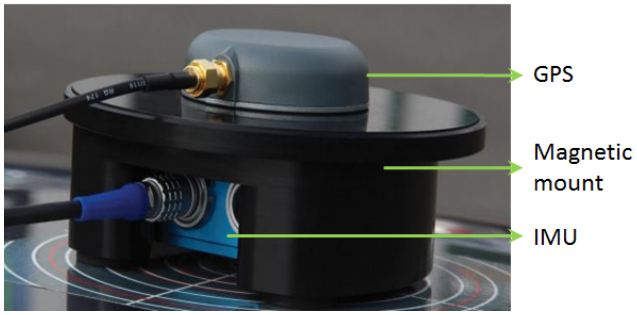

Fig. 4: GPS and IMU sensor set co-located with the magnetic mount

Vehicle Data using Controlled Area Network (CAN bus). A number of signals were also obtained by tapping into the vehicle CAN through the onboard data port of the Rav4EV. Since the vehicle is powered by the Tesla powertrain, the vehicle CAN network is an integration of V1-CAN from Toyota and EV-CAN from Tesla Motors. The V1-CAN consists of signals related to the vehicle such as accelerator pedal position and vehicle speed while EV-CAN consists of powertrain related signals such as motor speed, motor torque, DC voltage and battery state-of-charge (SOC).

3 Experimental Testing

Experimental testing of the Toyota Rav4EV was conducted on the Toyota Motor Manufacturing Canada (TMMC) test tracks. Fig. 5(a) shows the Rav4EV equipped up with the VMS. The Rav4EV was tested at TMMC test track as shown in Fig. 5 (b). Several straight line driving maneuvers, which included hard acceleration and hard braking, acceleration cruise and braking, coast down, and driving over a speed bump, were undertaken to excite the longitudinal dynamics of the vehicle. The VMS system was calibrated prior to testing. While few parameters such as wheel base, front and rear track widths are obtained directly from physical measurements and weight of the Rav4EV on each of the four wheels identified through weight scales at TMMC, all other model parameters were estimated based on track tests with the vehicle.

During coast down tests, wind speed was also recorded using a weather station. A brief summary of the road tests undertaken and parameters identified are given in Table 1.

Test type	**Vehicle Speed range**	**Parameters Identified**
Speed-bump test	Constant 15 Km/hr	Suspension parameters
Hard acceleration tests	0-100 Km/hr	Tire model parameters, Motor inertia, Wheel inertia, Motor model parameters
Acceleration and cruise tests	0-80 Km/hr 0-100 Km/hr	Position of center of gravity, Vehicle pitch inertia
Coast-down tests	0-70 Km/hr	Coefficient of drag and rolling resistance

Table 1: Experimental tests conducted

Journal of Computational and Nonlinear Dynamics. Received December 06, 2017;
Accepted manuscript posted July 16, 2018. doi:10.1115/1.4040870

Fig. 5: (a) Rav4EV fitted with VMS (b) TMMC test track

4 Parameter Identification

On-road testing was found to be a quick and reliable methodology for parameter identification. A two-stage optimization process was followed for parameter identification. Essentially, stage 1 was used to provide a good initial guess to stage 2 optimization. First, different mathematical models were considered to identify the individual parameters of the longitudinal plant model and control-oriented model. The parameters identified using this approach were thereafter optimized together using the full MapleSim vehicle dynamics model discussed in Section 5 and control-oriented models in Section 6 to obtain the final set of parameters.

Parameter Identification - Stage 1

In this section, we discuss the different equations of motion and mathematical models used for identifying the initial parameters of the longitudinal dynamics model of the Rav4EV. The data collected from different maneuvers has been processed

to estimate the required parameters.

A longitudinal dynamics model of the Rav4EV has been constructed considering a rigid chassis with no relative motion between the wheels and chassis. The dynamic equation for the longitudinal motion of the vehicle is expressed as:

$$M\dot{v} = F_x - F_r - F_d \tag{1}$$

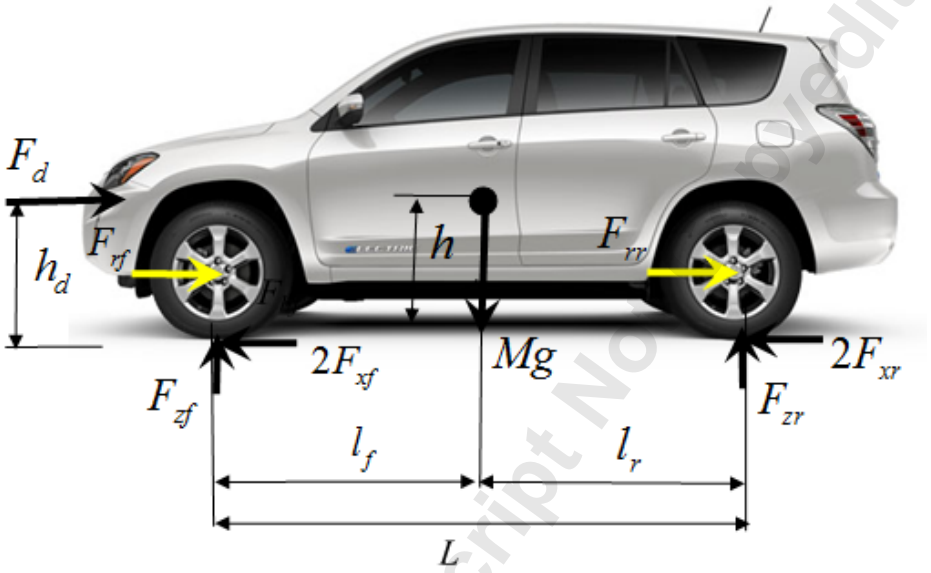

Fig. 6: Longitudinal forces acting on Rav4EV

where M represents the total mass of the vehicle, $F_x = 2F_{xf}$ is the sum of longitudinal traction/braking forces acting on the each of the front wheels ($F_{xr} = 0$ for a front wheel driven vehicle), $F_r = F_{rf} + F_{rr}$ is the rolling resistance force on the front and rear wheels and F_d is the aerodynamic drag force acting at the center of pressure h_d. F_{zf} is the sum of normal forces on the front wheels and F_{zr} is the sum of normal forces on the rear wheels and L is the wheel base indicating the distance between the front and rear wheels. The longitudinal distance of center of gravity (CG) from front and rear wheels are l_f and l_r respectively, while the vertical distance of CG from ground is represented by h. The forces acting on the Rav4EV during longitudinal motion are shown in Fig. 6. The parameters to be determined have been categorized as follows:

4.1 Parameters for longitudinal force

The longitudinal force F_x is the sum of longitudinal traction/braking forces acting on the front and rear wheels. Since the Rav4EV is a front wheel driven vehicle, the traction force on the rear wheels is considered negligible. The longitudinal force is a function of road load assumed to be governed by Pacejka's Magic formula tire model. The normal force distribution between front and rear wheels varies as a result of pitching during acceleration and braking. In the following section, we

determine the Pacejka tire model parameters, position of center of gravity, and pitch inertia of the vehicle and suspension stiffness, and damping parameters.

4.1.1 Tire model parameters

The longitudinal force generated at each tire is a function of longitudinal slip ratio and the normal force applied on the tires. For a front wheel drive vehicle, the traction force on the two front wheels is represented as:

$$F_x = 2F_{xf} = 2\mu(\lambda)F_{zf} \tag{2}$$

where μ is the normalized longitudinal force governed by the Pacejka tire model [11] which is a function of the slip ratio λ. The slip ratio for an accelerating wheel is defined as:

$$\lambda = \frac{r_{eff}\omega_w - v}{r_{eff}\omega_w} \tag{3}$$

where ω_w is the angular velocity of the wheel, r_{eff} is the dynamic radius of the wheel and v is the vehicle speed. The relationship between μ and λ is represented by Pacejka's Magic formula tire model as:

$$\mu = D\sin\left[C\tan^{-1}\left\{B\lambda - E\left(B\lambda - \tan^{-1}B\lambda\right)\right\}\right] \tag{4}$$

The parameters of Pacejka's Magic formula tire model in equation (4) are determined by plotting μ with the longitudinal slip ratio λ. Using a non-linear curve fit, the parameters of the Magic formula tire model as seen in Fig.7 have been estimated as B=49, C=1.37, D=1.25 and E=0.01. The model parameters B, C, D and E in equation (4) are:

B: Stiffness factor. It determines the slope at the origin

C: Shape factor. It determines the range of the sine function

D: Peak value. It represents the peak value of the tire force.

BCD: The product of BCD represents the longitudinal stiffness of the tire.

E: Curvature factor. It is used to represent the curvature near the peak of the curve.

4.1.2 Pitch inertia and Position of center of gravity

The pitch inertia (I_y), position of longitudinal center of gravity (CG) (l_r or l_f) and height of CG (h) are identified by exciting the pitching motion of the vehicle through rapid acceleration and hard braking tests. The data gathered on front and

Journal of Computational and Nonlinear Dynamics. Received December 06, 2017;
Accepted manuscript posted July 16, 2018. doi:10.1115/1.4040870

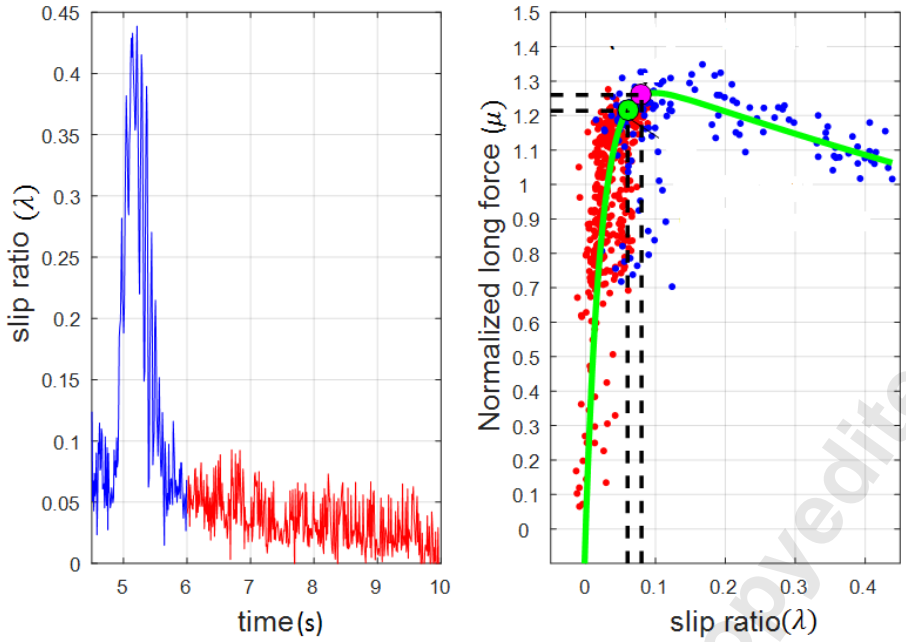

Fig. 7: (a) Slip ratio λ vs time (b) Normalized longitudinal force μ vs λ

rear tires during acceleration/braking maneuvers is processed to obtain these parameters. The equation governing the pitch motion of the vehicle is expressed as:

$$I_y\ddot{\theta} = -F_{zf}l_f + F_{zr}l_r - M\dot{v}h \tag{5}$$

where, I_y is the pitch inertia of the vehicle and $\dot{v}$ is the acceleration at the center of gravity of the vehicle. Rearranging the terms to obtain normal force on the front wheels:

$$F_{zf} = \frac{Mgl_r}{L} - \frac{Mh\dot{v}}{L} - \frac{I_y\ddot{\theta}}{L} \tag{6}$$

Since the GPS is not positioned at the CG of the vehicle but at the roof of the car, the acceleration recorded by the GPS needs to be transformed to the CG of the vehicle. Neglecting the small centripetal terms, the longitudinal vehicle acceleration at CG is expressed as:

$$\dot{v} = \dot{v}_{GPS} + \ddot{\theta}(h - H) \tag{7}$$

where H is the height at which GPS is mounted from the ground. Substituting equation (7) into (6), we have:

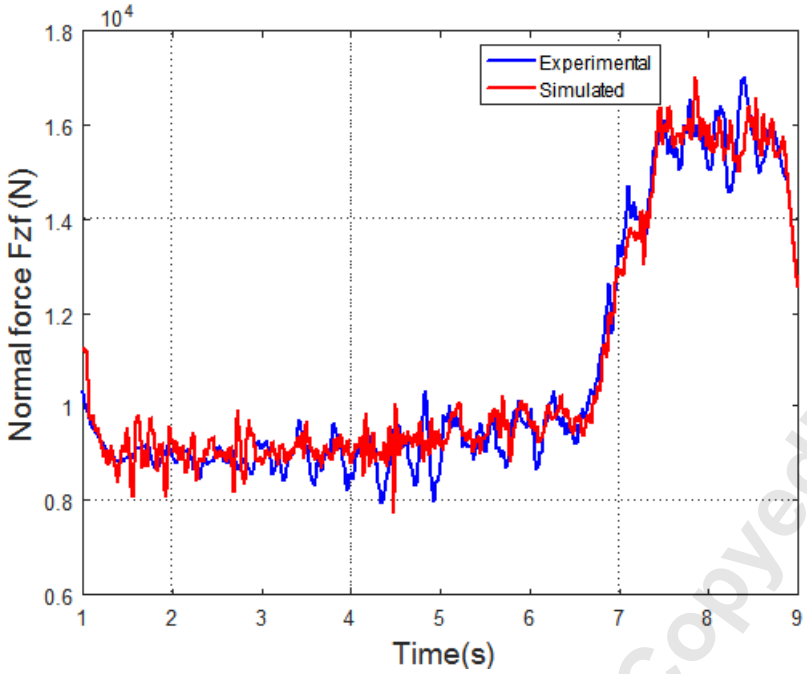

Fig. 8: Experimental vs estimated normal force

$$F_{zf} = \frac{Mgl_r}{L} - \frac{Mh(\dot{v}_{GPS} + \ddot{\theta}(h-H))}{L} - \frac{I_y\ddot{\theta}}{L} \tag{8}$$

where the vehicle acceleration in longitudinal direction ($\dot{v}_{GPS}$) is measured using the GPS, and pitch acceleration ($\ddot{\theta}$) measured by taking a derivative of the pitch rate measured by the IMU. By minimizing the difference between the experimental and simulated normal force on the front wheels (F_{zf}), as shown in Fig 8, the parameters have been estimated as $I_s = 3052\ kgm^2$, $l_r = 1.42\ m$ and $h = 0.62\ m$.

4.1.3 Parameters for Suspension

The front suspension of the Rav4EV is a Mcpherson strut while the rear suspension is of double wishbone type. To include load transfer effects due to pitching motion of the vehicle during acceleration and braking maneuvers, we have considered a simplistic approach of modeling the front and rear suspensions as linear spring and damper elements and assumed that the suspension elements are symmetric about the longitudinal axis for left/right wheels. We consider a four-DOF half car model as shown in Fig. 9, with the aim to estimate the stiffness parameters (K_f, K_r) and damping parameters (C_f, C_r) of front and rear suspensions. The model allows vertical motion (z direction) and pitch motion (θ) of the car chassis (sprung mass) and vertical motions of the front and rear wheels (z_{ft}, z_{ft}). The sprung mass (M_s) is calculated by subtracting the half car mass from those of the two wheels (M_{tf}, M_{tr}) and the pitch inertia (I_s) of the sprung mass is calculated by

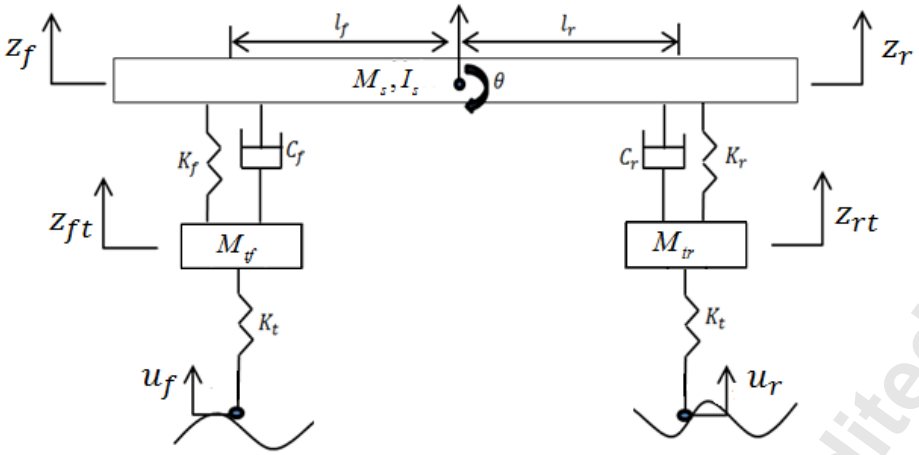

Fig. 9: 4-DOF car model for identification of suspension parameters

subtracting half the vehicle inertia ($\frac{I_y}{2}$) of the from the inertia of the unsprung mass (I_u) about the CG as follows:

$$\begin{aligned} M_s &= \frac{M}{2} - (M_{tf} + M_{tr}) \\ I_s &= I_y - I_u \end{aligned} \tag{9}$$

where $I_y = F_{zf} l_f^2 + F_{zr} l_r^2$ and $I_u = M_{tf} l_f^2 + M_{tr} l_r^2$. The tires are modelled as linear springs with stiffness K_t. Since the damping of the tires is small as compared to that of the suspension elements, it is neglected. The equations of motion for M_s and I_s for a vehicle driven at a constant speed v are:

$$\begin{aligned} M_s \ddot{z} = &- \overbrace{K_f \{z_f - z_{tf}\} - C_f \{\dot{z}_f - \dot{z}_{tf}\}}^{F_{zf}} \\ &- \overbrace{K_r \{z_r - z_{tr}\} - C_r \{\dot{z}_r - \dot{z}_{tr}\}}^{F_{zr}} \end{aligned} \tag{10}$$

$$\begin{aligned} I_s \ddot{\theta} = &l_f \left[K_f \{z_f - z_{tf}\} + C_f \{\dot{z}_f - \dot{z}_{tf}\}\right] - \\ &l_r \left[K_r \{z_r - z_{tr}\} + C_r \{\dot{z}_r - \dot{z}_{tr}\}\right] \end{aligned}$$

The equations of motion for unsprung masses (M_{tf}) and (M_{tr}) consisting of the wheel and suspension mass can be

written as:

$$\begin{aligned} M_{tf}\ddot{z}_{tf} &= K_f\{z_f - z_{tf}\} + C_f\{\dot{z}_f - \dot{z}_{tf}\} - K_t(z_{tf} - u_f) = 0 \\ M_{tr}\ddot{z}_{tr} &= K_r\{z_r - z_{tr}\} + C_f\{\dot{z}_r - \dot{z}_{tr}\} - K_t(z_{tr} - u_r) = 0 \\ z_f &= z + l_f\cos\theta \qquad \text{and} \qquad z_r = z - l_r\cos\theta \end{aligned} \tag{11}$$

The input to the model is a speed bump of a known profile to excite pitch and heave motions. The road profile inputs u_i to the model can be expressed as:

$$u_i = \frac{A}{2}\left[\begin{cases} 0 & t < \frac{D_i}{v} \\ 1 - \cos(\frac{2\pi}{\lambda_{bump}}D_i) & \frac{D_i}{v} \le t \le \frac{D_i+\lambda_{bump}}{v} \\ 0 & t > \frac{D_i+\lambda_{bump}}{v} \end{cases}\right] \tag{12}$$

where $A = 0.072\ m$ is the height of the speed bump, $\lambda_{bump} = 49.5\ mm$ is the length of the speed bump and D_i is the distance taken by the front or rear tire to travel to the speed bump and $i = f, r$ refers to the front and rear tire respectively.

The suspension parameters are determined by minimizing the cost function J expressed as:

$$J = \int_0^t \left[w_1 {J_1}^2 + w_2 {J_2}^2 + w_3 {J_3}^2\right] dt \tag{13}$$

where J_1, J_2, and J_3 are the costs with respect to normal forces (F_{zf} and F_{zr}) on the front and rear wheels and pitch rate ($\dot{\theta}$) of the unsprung mass, expressed as:

$$\begin{aligned} J_1 &= F^*_{zf} - \overbrace{(M_{sf} + M_{tf})g + K_t(z_{tf} - u_f)}^{F_{zf}} \\ J_2 &= F^*_{zr} - \overbrace{(M_{sr} + m_{tr})g + K_t(z_{tr} - u_r)}^{F_{zr}} \\ J_3 &= \dot{\theta}^* - \dot{\theta} \end{aligned} \tag{14}$$

where F^*_{zf}, F^*_{zr} and $\dot{\theta}^*$ are the experimentally measured normal force on the front wheel, normal force on the rear wheel and pitch rate, and w_1, w_2, and w_3 are the corresponding weights. A comparison of the experimental and simulated suspension forces is given in Fig. 10. Using the non-linear least square algorithm, the suspension parameters have been identified as

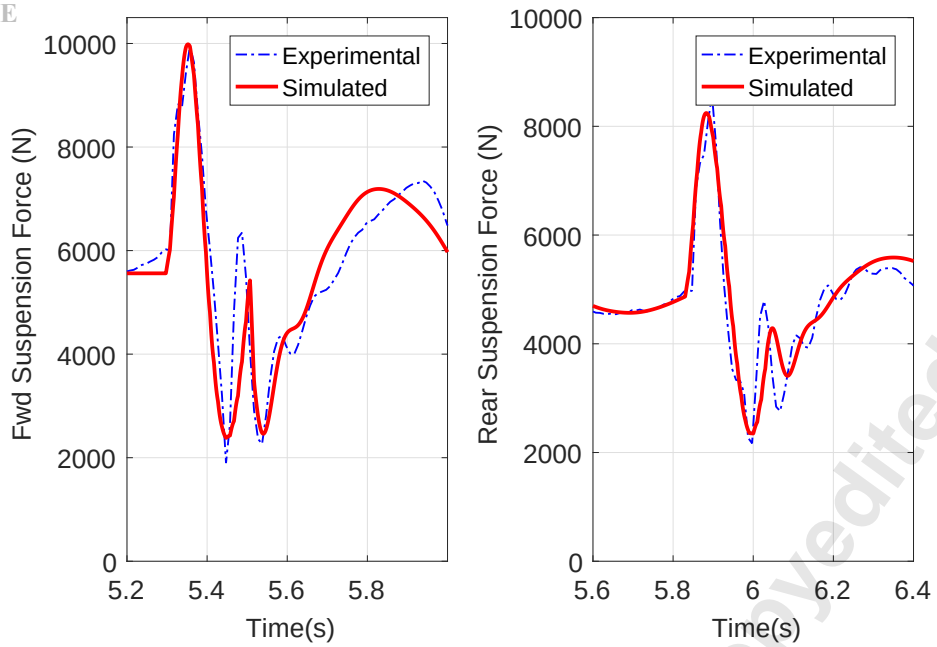

Fig. 10: Normal force on the front left and rear left wheels

$K_f = 54,370\ N/m$, $K_r = 35,540\ N/m$, $C_f = 1980\ Ns/m$ and $C_r = 1795\ Ns/m$. The vertical tire stiffness (K_t) is assumed to be $253,000\ N/m$ as given in the manufacturer's specifications.

4.2 Resistance force parameters

The forces resisting the longitudinal motion of the vehicle are the aerodynamic drag force and the rolling resistance force. Aerodynamic drag force (F_d) is the force due to the air resistance acting on the frontal area of the vehicle. This can be represented as:

$$F_d = \frac{1}{2}\rho C_d A_f v^2 \tag{15}$$

where ρ is the density of air, assumed as $1.2 Kg/m^3$. The parameters estimated are the aerodynamic drag coefficient C_d and the frontal area of the vehicle A_f. The rolling resistance force is caused by a non-symmetric distribution of normal tire load over the contact patch. The rolling resistance force F_r at the tire center can be modeled as:

$$F_r = f_{rr}(F_{zf} + F_{zr}) \tag{16}$$

where f_{rr} is the rolling resistance coefficient to be estimated.

4.2.1 Frontal area and Center of pressure

Frontal area of a vehicle is the orthogonal projection of the vehicle on a plane perpendicular to the longitudinal axis of the vehicle. Frontal area is an important parameter that determines the aerodynamic drag, thus affecting the power consumption of the vehicle. In this research work, the frontal area (A_f) is estimated using an image processing technique [12]. The frontal

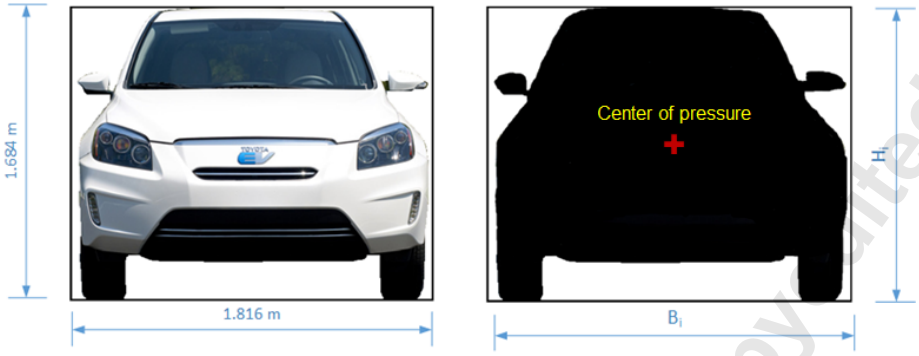

Fig. 11: Frontal area of Rav4EV and processed image with black and white pixels

image of the Rav4EV was processed to fill the car area with black color and background with white color. Then '**im2bw**' function in the Image Processing Toolbox of MATLAB is used to convert the grey scale image to binary image. The grey scale image's darker pixels are replaced by 0 and lighter pixels are replaced by 1 in the final binary image as shown in Fig 11. Counting the pixels ($B_i \times H_i$) of the black and white color, the actual frontal area of Rav4EV has been calculated as 2.464 m^2 which is 80.6% of the total area of the box (3.058 m^2).

Further, assuming uniform air pressure distribution over the frontal area, the centroid of the figure could represent the center of pressure where the aerodynamic drag force acts. The height of center of pressure (h_d) has been estimated as 0.689 m.

4.2.2 Coefficient of drag and rolling resistance

The aerodynamic drag coefficient (C_d) is determined from a coast-down test in accordance with the methodology followed by White and Krost [13]. The Rav4EV was accelerated to about 65 Km/hr, and then the throttle was released, so that the vehicle slows down under the effects of aerodynamic drag and rolling resistance. The vehicle speed recorded with and against the wind can be seen in Fig. 12.

During coast-down, the traction force (F_x) on the vehicle is small and therefore neglected. The longitudinal dynamics equation (1) reduces to:

$$M\dot{v} = \frac{1}{2}\rho C_d A_f v^2 + F_r$$

$$or \tag{17}$$

$$-\frac{dv_x}{\frac{\rho C_d A_f v_x^2}{2M} + \frac{F_r}{M}} = dt$$

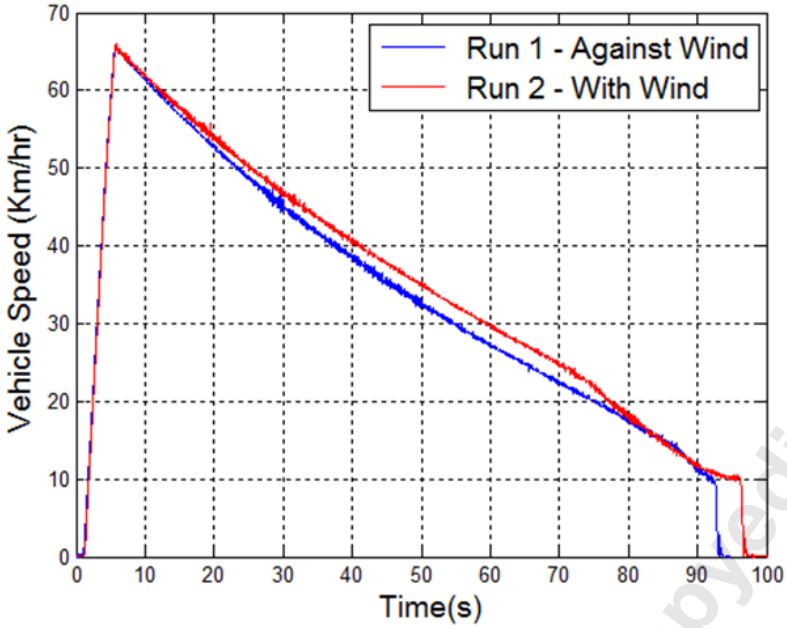

Fig. 12: Vehicle speed recorded during coast down testing of Rav4EV

where F_r is assumed to be constant for speeds below 70 Km/hr [13]. Integrating equation (17), assuming an initial velocity of v_i, the coast down time t for vehicle speed to drop from v_i to v_x can be expressed as:

$$\frac{t}{T} = 1 - \frac{\tan^{-1}\left[v_x\left(\frac{\rho C_d A_f}{2F_r}\right)^{\frac{1}{2}}\right]}{\tan^{-1}\left[v_i\left(\frac{\rho C_d A_f}{2F_r}\right)^{\frac{1}{2}}\right]} \tag{18}$$

Solving for velocity v_x from equation (18) yields:

$$v_x = \left(\frac{2F_r}{\rho C_d A_f}\right)^{\frac{1}{2}} \tan\left\{\left(1 - \frac{t}{T}\right)\tan^{-1}\left[v_i\left(\frac{\rho C_d A_f}{2F_r}\right)^{\frac{1}{2}}\right]\right\} \tag{19}$$

Simplifying further,

$$\frac{v_x}{v_i} = \frac{1}{\beta}\tan\left[\left(1 - \frac{t}{T}\right)\tan^{-1}\beta\right] \tag{20}$$

where

$$\beta = v_i \left(\frac{\rho C_d A_f}{2F_r} \right)^{\frac{1}{2}} \tag{21}$$

The parameter β is estimated from (20) by plotting non-dimensional velocity ($\frac{v_x}{v_i}$) against non-dimensional time ($\frac{t}{T}$) as shown in Fig. 13.

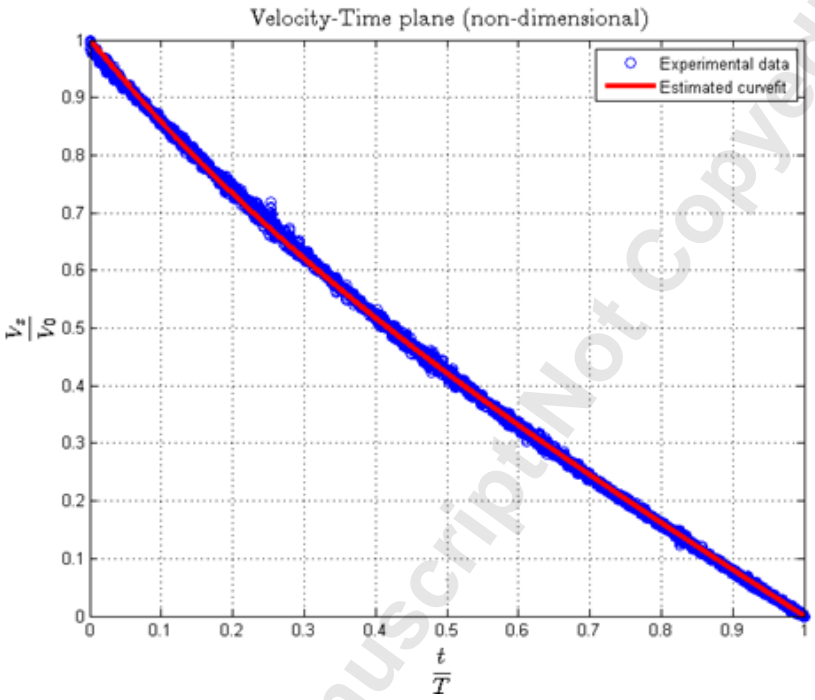

Fig. 13: Plot of $\frac{v_x}{v_0}$ against $\frac{t}{T}$ to estimate β

The coefficient of drag C_d is obtained as:

$$C_d = \frac{2M\beta \tan^{-1}\beta}{v_i T \rho A_f} \tag{22}$$

and coefficient of rolling resistance f_{rr} is obtained as:

$$f_{rr} = \frac{v_i \tan^{-1}\beta}{\beta T g} \tag{23}$$

From data collected over 5 runs, the average coefficient of drag (C_d) was estimated as 0.308 which is close to 0.3

specified in the Toyota technical manual. The average coefficient of rolling resistance (f_{rr}) was estimated as 0.0015.

4.3 Inertia and halfshaft parameters

The inertial parameters for the motor, transmission, wheels, and halfshaft stiffness and damping are required to estimate the time delays between demanded and achieved torque. The inertial properties also determine the driveline oscillation characteristics and govern the wheel torque transmitted from the drivetrain to the wheels.

4.3.1 Drivetrain inertia

The powertrain of the Rav4EV consists of a central motor driving the wheels through a single reduction gear. A differential connects the two front wheels on either side of the motor. The dynamics of the motor and gearbox, and those of gearbox and halfshaft can be represented as:

$$J_m \dot{\omega}_m = \frac{T_m}{\eta_t} - \frac{T_t}{gr} \tag{24a}$$

$$J_t \dot{\omega}_t = T_t - T_w \tag{24b}$$

where J_m represents motor inertia, J_t transmission inertia, η_t efficiency of transmission, gr gear ratio of transmission and T_t transmission torque. Combining equations (24a) and (24b), the equation for drivetrain dynamics can be written in terms of measured motor torque (T_m) and wheel torque (T_w) as:

$$\underbrace{\left(J_m + \frac{J_t}{gr^2}\right)}_{J_d} \dot{\omega}_m = \frac{T_m}{\eta_t} - \frac{T_w}{gr} \tag{25}$$

which was used to simulate angular speed of motor (ω_m) for measured inputs T_m and T_w.

By comparing the experimental and simulated motor speed (ω_m) as shown in Fig. 14, the combined drivetrain inertia (J_d) has been estimated as 0.423 kgm^2 and drivetrain efficiency as 94.6%.

4.3.2 Wheel inertia

A free body diagram (FBD) of the forces acting on the driven wheel is shown in Fig. 15. The dynamic equation governing the driven wheel dynamics can be expressed as:

$$J_w \dot{\omega}_w = T_w - r_{eff} F_{xf} - M_{rr} \tag{26}$$

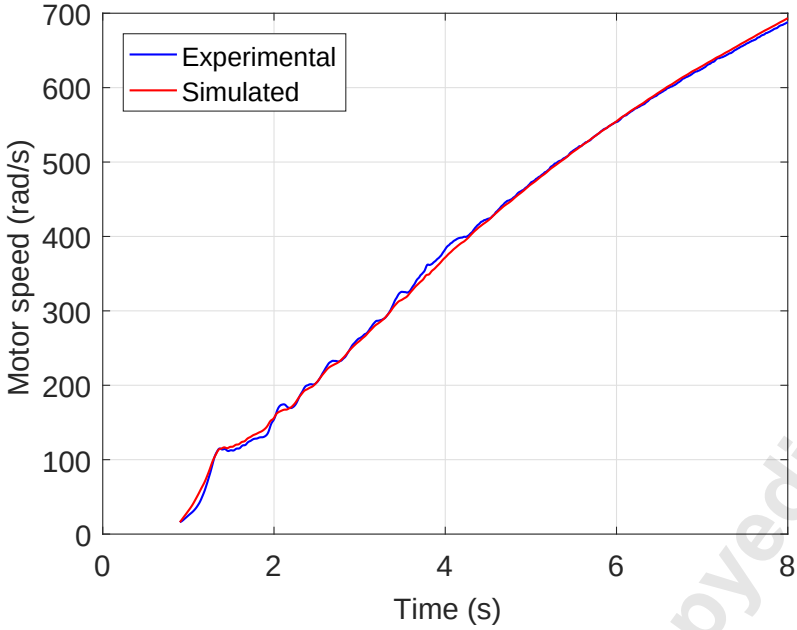

Fig. 14: Experimental vs simulated motor angular speed (ω_m)

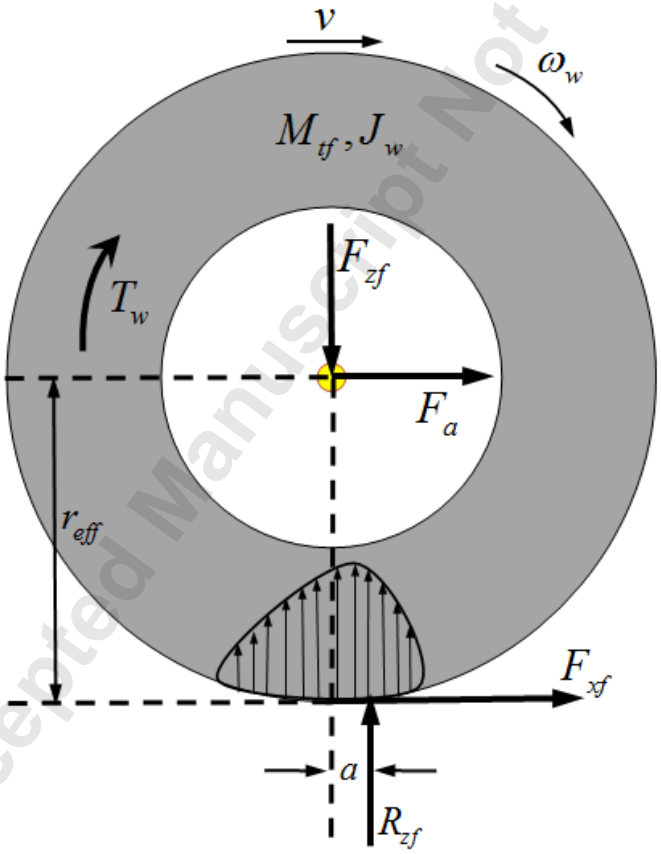

Fig. 15: Free-body diagram showing forces on the front (driven) wheel

where $\dot{\omega}_w$ is the angular acceleration of wheel, r_{eff} is the measured dynamic radius of the wheel, and rolling resistance moment is $M_{rr} = aR_{zf} = f_{rr}F_{zf}$. The rolling resistance coefficient (f_{rr}) is estimated as 0.0015 (section 4.2.2) and mass of the wheel (M_{tf}) including rims with tire specification $225/65\ R17$ was measured as 22.7 kg. The relation between the

longitudinal force (F_{xf}) at the ground and force F_a measured by the VMS at the centre of the wheel hub is expressed as:

$$F_{xf} = M_{tf}\dot{v} - F_a \tag{27}$$

By comparing the experimental and simulated wheel speed (ω_w) as shown in Fig. 16, the wheel inertia (J_w) has been estimated as 2.72 kgm^2.

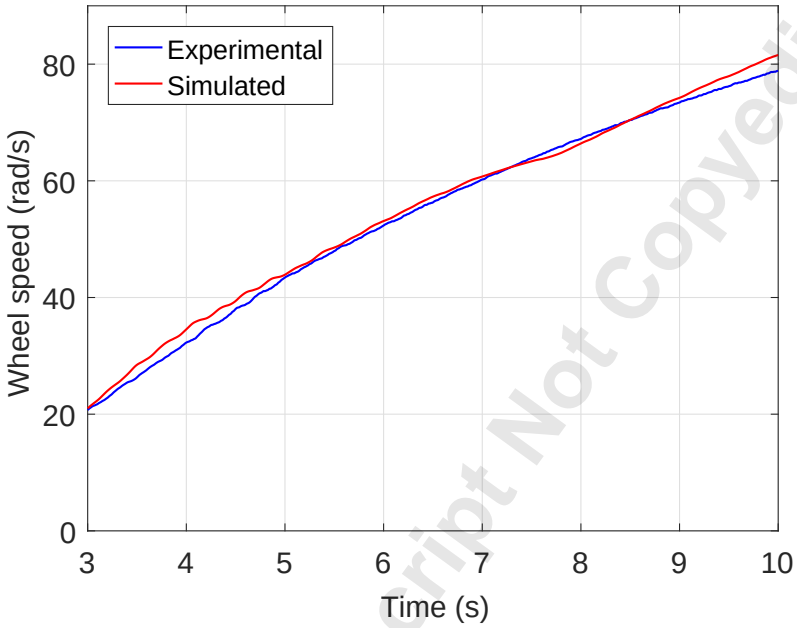

Fig. 16: Experimental and simulated wheel spin (ω_w)

4.3.3 Parameters for halfshaft

Halfshafts are used to transmit the transmission torque from the gearbox to the wheel. The halfshaft is modeled as a torsional spring and damper system (1 DOF) negligible inertia. The stiffness of these shafts was derived from the physical and material properties of the halfshaft obtained from the manufacturer drawings. Torsional stiffness (torque required per unit twist) of the shaft is expressed as:

$$k = \frac{GJ_{hs}}{L_{hs}} \tag{28}$$

where G is the modulus of rigidity, J_{hs} is the polar moment of inertia and L_{hs} is the length of shaft. As the halfshaft has three different diameters over its length, the equivalent stiffness k is calculated by summing the longitudinal stiffness of each section. The torsional stiffness k of the halfshaft is calculated as 22555 Nm/rad. The damping parameter of the halfshaft c

is chosen as 200 $Nm/rad/s$ as in [14], which is typical for halfshafts of similar length and diameters.

5 Plant Model for longitudinal dynamics

In this research, MapleSim, a software based on graph-theoretic modeling [15], is used to create a longitudinal dynamics model of the Rav4EV. MapleSim can be used to generate highly optimized simulation code useful for real-time implementation. MapleSim provides a library of standard components such as rigid bodies, springs, dampers, joints and tires which can be combined to create highly customized models for a user-application. The developed models are acausal, which means that they are adaptable to the direction of data flow unlike traditional input/output blocks.

A full-car chassis model of the front wheel drive Rav4EV with 18 DOF has been developed in MapleSim. The chassis has 6 DOF, wheels 4 DOF, suspension 4 DOF and halfshaft 4 DOF. The tires have been modeled using Pacejka's Magic formula relaxation length model so that the effect of wheel slip transients are included. The model consists of a rigid body representing the car mass, connected to both front and rear tires through suspensions. Both suspensions are simplistically modeled as linear spring dampers which allow only vertical displacement. The motor torque is amplified in a single-reduction gearbox and applied to the forward wheels through a halfshaft. The halfshaft is modeled as a torsional spring and damper system of negligible mass (being small). The halfshaft is connected on both the wheel and the gearbox sides with universal joints with an additional prismatic joint on the wheel side to cater for any lateral movement of the forward wheel. A representation of the full-car longitudinal dynamics model in MapleSim is shown in Fig. 17.

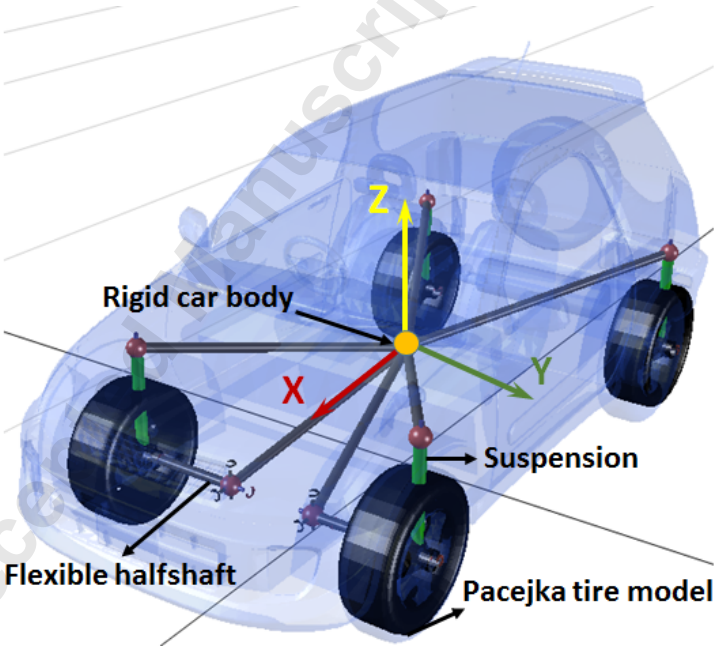

Fig. 17: Full-car longitudinal dynamics model of Rav4EV in MapleSim

The various model components are explained in detail as follows:

(a) **Vehicle chassis**. In the MapleSim model, the vehicle chassis is modeled as rigid body with mass, CG and inertia

parameters specified for the rigid body. The rigid car body is connected to the front and rear suspensions through a rigid body frame that defines the position and orientation relative to the center of gravity.

(b) **Suspension components**. Suspension elements connect the car mass to the front and rear wheels. The suspension elements are modeled using prismatic joints that exhibit linear stiffness and damping characteristics. The prismatic joint allows relative translational motion between the wheel and vehicle chassis only in the vertical direction. The prismatic joint is assumed to have an initial displacement due to the weight of chassis acting on the spring. Each prismatic joint is connected to the wheel through a revolute joint, thus allowing the wheel one rotational degree of freedom. The stiffness and damping parameters of this revolute joint are assumed to be zero to simulate an ideal joint.

(c) **Tire components**. Each tire consists of two sub-components; a standard tire body and a tire model. The standard tire component computes the kinematic parameters such as slip angle, slip ratio and dynamic tire radius based on vertical tire stiffness and load changes on application of a normal load on the tire. The parameters of the standard tire component are tire mass, tire inertia, vertical stiffness, damping and unloaded tire radius. MapleSim has a library of different tire models (Linear, Fiala, Calspan, Pacejka, and user-defined) to calculate the forces and moments acting at the contact patch. In this research, we have used a user-defined tire model. The longitudinal force to be input in the tire model are computed by developing custom components based on the Pacejka tire model as given in equation (4) while the normal force is computed directly from the standard tire component.

(d) **Half shaft components**. Half shaft is modeled as a torsional spring and damper system. The halfshaft has universal joints at each end. One end of the halfshaft is connected to the powertrain while the other end is connected to the wheel. An ideal prismatic joint is also added between the halfshaft and wheel to allow for any lateral displacement of the wheel.

The model accepts motor torque (T_m) as an input and outputs halfshaft (wheel) torque (T_{hs}), vehicle speed (v), and wheel speed ($Wh_{sp} = r_{eff}\omega_w$). The model was exported as an optimized S-function so that it could be used for simulation and control in Matlab/Simulink.

6 Control-Oriented Models

A reduced control-oriented model is required to enable real-time implementation within a controller. A central motor connects to the two forward wheels through a gearbox and flexible shafts, which in turn connect to the wheels. A powertrain model for a front-wheel drive EV with a central drivetrain is shown in Fig. 18. Since the powertrain is symmetric about each of the forward wheels, the equations of motion have been derived for only one half of the powertrain. In this model, J_m and J_t represent half the inertia of the motor and transmission and J_w, the inertia of the wheel. The halfshaft is modeled as a torsional spring and damper with stiffness k and damping c. The inertia of the halfshaft is neglected since it is small as compared to the mass of the vehicle. The mass of the vehicle is represented as M, reduction ratio of the gearbox as gr, dynamic radius of the wheel as r_{eff} and torsion angle in the halfshaft as $\frac{\theta_m}{gr} - \theta_w$.

In general, powertrain models for anti-jerk control are based on either halfshaft torsion control or wheel slip ratio control. In this research, we have combined the two approaches for better anti-jerk performance.

Journal of Computational and Nonlinear Dynamics. Received December 06, 2017;
Accepted manuscript posted July 16, 2018. doi:10.1115/1.4040870

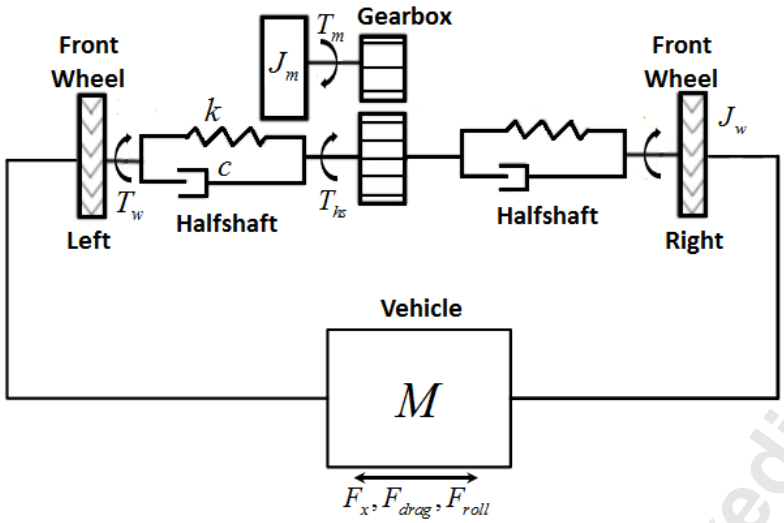

Fig. 18: Vehicle powertrain model

6.1 Model based on halfshaft torsion control

The vehicle can be modeled as a two-inertia system [16], where the inertia of vehicle and the wheel is lumped on one side while the inertia of the motor and transmission is lumped on the other side. In this model, it is assumed that a tire is a rigid body, and its inertia is added to that of the vehicle. The halfshaft is modeled as a torsional spring and damper connecting the two inertias. A diagram representing the system is shown in Fig 19. The dynamic equation representing the motor and

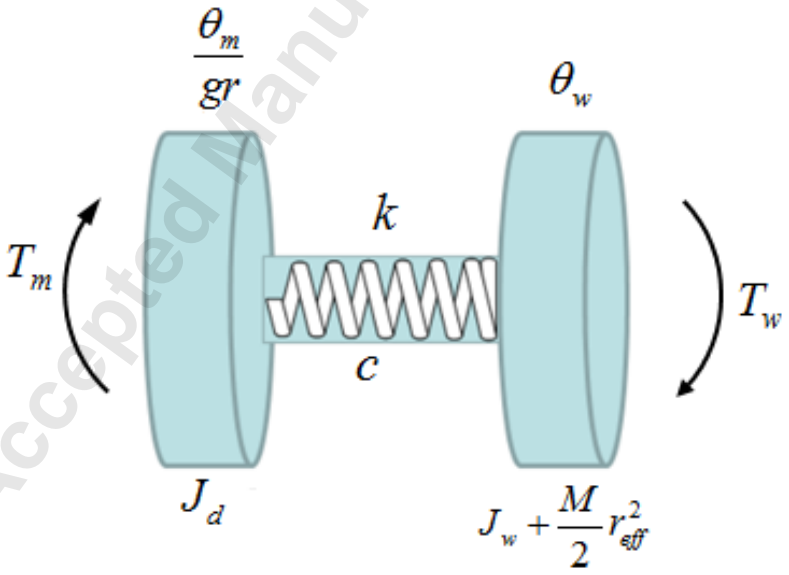

Fig. 19: Diagram of the EV powertrain

transmission dynamics for a single front wheel is:

$$J_d\dot{\omega}_m = T_m - \underbrace{\frac{k}{gr}(\frac{\theta_m}{gr} - \theta_w) - \frac{c}{gr}(\frac{\omega_m}{gr} - \omega_w)}_{\frac{T_{hs}}{gr}} \tag{29}$$

where T_m is the motor torque, T_{hs} is the halfshaft torque, ω_m is the angular velocity of the motor, ω_w the angular velocity of the wheel and drivetrain inertia is given by:

$$J_d = J_m + \frac{J_t}{gr^2} \tag{30}$$

The wheel dynamics can be represented as:

$$J_w\dot{\omega}_w = T_w - r_{eff}\frac{F_x}{2} - f_{rr}F_{zf} \tag{31}$$

The vehicle acceleration ($\dot{v}$) is:

$$M\dot{v} = F_x - F_d - F_r \tag{32}$$

Since the tire is assumed to be rigid, the vehicle acceleration can be related to angular wheel acceleration as $\dot{v} = r_{eff}\dot{\omega}_w$. The traction force ($F_x$) in equation (32) can therefore be represented as:

$$F_x = Mr_{eff}\dot{\omega}_w + F_d + F_r \tag{33}$$

Substituting for F_x in the equation (31), the wheel and vehicle dynamics are given by:

$$(J_w + \frac{M}{2}r_{eff}^2)\dot{\omega}_w = T_w - r_{eff}\frac{F_r}{2} - r_{eff}\frac{F_d}{2} \tag{34}$$

Combining equations (29) and (34), the system model representing the dynamics of the powertrain is formulated with states as: $x = \begin{bmatrix} \frac{\theta_m}{gr} - \theta_w & \omega_m & \omega_w \end{bmatrix}^T$, input $u = T_m$, and outputs $Y = \begin{bmatrix} T_{hs} & v \end{bmatrix}^T$.

6.2 Model based on halfshaft torsion and wheel slip control

The model discussed in section 6.1 considers the tire as a rigid body; thus it assumes that the longitudinal force applied to the wheel is transmitted to the tire (33). However, the longitudinal force acting on the tires is a function of the tire-road friction. Therefore, a more realistic vehicle model, that includes the tire flexibility and tire-road friction effects has been formulated. This model will help control wheel-slip during sudden changes in driver torque demand, in addition to halfshaft torsion, or during changes in road condition.

The equations for motor/transmission dynamics (29) and (30), wheel dynamics (31) and vehicle acceleration (32) for this wheel-slip based model is the same as that for the halfshaft torsion model. However, the simplistic longitudinal force model (33) for the halfshaft torsion model is replaced with linear or non-linear tire models. Several tire models like Lugre [17], Burckhardt [18], Kiencke and Dias [19] and Pacejka 2002 [20] have been used to model tire-road friction. Out of the these, we have used the Pacejka 2002 tire model, since parameters have been identified for this model.

Slip-based transients play an important role in driveline oscillations especially during tip-in and tip-out maneuvers. Since our aim is to develop models for anti-jerk control, we have modeled slip based transients based on Pacejka's relaxation length model [21]. The dynamic equation for transient slip λ_t can be expressed as:

$$\dot{\lambda}_t = \frac{r_{eff}\omega_w}{Rl} - \frac{v}{Rl} - \frac{v}{Rl}\lambda_t \tag{35}$$

where (Rl) is defined as the distance needed by the tire to reach a certain percentage of the steady state slip with a step change in slip. The longitudinal relaxation length (Rl) of the tire is assumed as 0.3 as in [22]. To avoid singularities close to 0 speed as discussed in [23], we linearize equation (35) about an operating speed v_{op}:

$$\dot{\lambda}_t = \frac{r_{eff}\omega_w}{Rl} - \frac{v}{Rl} - \frac{v_{op}}{Rl}\lambda_t \tag{36}$$

A comparison of the wheel slip response in the halfshaft torsion control model and the transient-slip model with respect to experimental slip can be seen in Fig. 20. It can be observed in the plot that while halfshaft control model does not exhibit slip-based oscillations, the transient-slip model shows slip-based oscillations as it is based on more realistic assumption of tire slip. There are still some differences between wheel slip oscillations between experimental and transient-slip model, since the transient-slip model is based on a simplified assumption of constant wheel radius. However, the slip-based control model serves the purpose of including the tire-slip effects, which are generally ignored in the halfshaft torsion model.

Including the effect of slip-based transients, the longitudinal force on each tire based on Pacejka non-linear tire model and linear tire model is:

(a) **Pacejka tire model**: Based on equation (4):

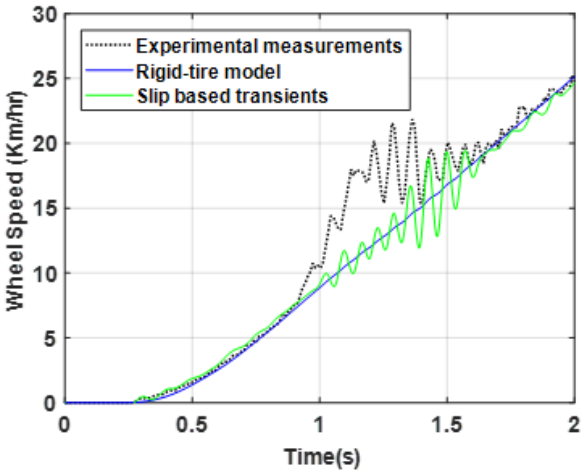

Fig. 20: Comparison of slip-based transients in halfshaft torsion model and transient-slip model against experiments

$$F_x = D\sin\left[C\tan^{-1}\left\{B\lambda_t - E\left(B\lambda_t - \tan^{-1}B\lambda_t\right)\right\}\right]F_{zf} \tag{37}$$

where parameters B, C, D, and E are experimentally identified as discussed in section 4.1.1. The normal load F_{zf} on each of the front wheels based on equation (6) is calculated as:

$$F_{zf} = \frac{M}{2L}(gl_r - h\dot{v}) \tag{38}$$

The pitch acceleration $\ddot{\theta}$ for a straight line maneuver is small and therefore neglected.

(b) **Linear tire model**: The longitudinal force is given by:

$$F_x = C_t\lambda_t \tag{39}$$

where the transient longitudinal stiffness $C_t = C_x Rl$, and the longitudinal stiffness $C_x = (BCD)F_{zf}$.

Combining equations (29) to (32) and (36) to (38)/(39), a model for anti-jerk or driveline oscillation control of EVs is formulated with states as: $x = \begin{bmatrix} \omega_m & \omega_w & v & \theta_m & \theta_w & \lambda_t \end{bmatrix}^T$, input: T_m, disturbance inputs: $\begin{bmatrix} -F_r & -F_d & -v_{op} \end{bmatrix}^T$, and outputs: $\begin{bmatrix} T_{hs} & v & Wh_{sp} \end{bmatrix}^T$.

Difference in Pacejka and Linear tire models

The longitudinal force approximated using the Pacejka tire model (37) and that by the linear tire model (39) has been compared in Fig. 21. It can be seen that initially, there is no major difference in the rate of increase of longitudinal force with

slip. However, at slip ratios higher than 0.035, the longitudinal force approximated by the linear tire model is marginally higher as compared to that recorded by the Pacejka tire model. It can also be seen that the longitudinal force for the Rav4EV saturates at 5300 N, when a slip ratio of 0.062 is reached. The control bounds for longitudinal force and slip can accordingly be defined below these limits.

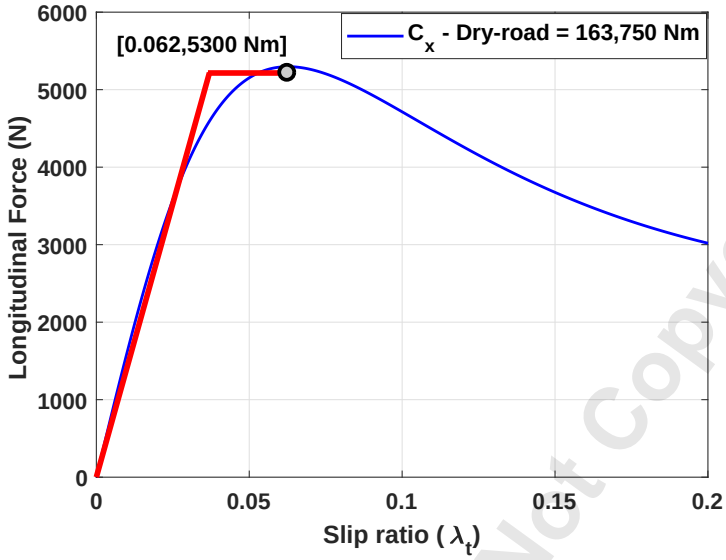

Fig. 21: Comparison of longitudinal force vs wheel slip in linear and Pacejka tire models

While Pacejka tire model estimates the longitudinal force more accurately than a linear tire model, it will result in a higher computation time. The control design is a choice between accuracy and computation time. The real-time implementation capability with MPC-based controller based on both linear and Pacejka tire models has been demonstrated in [24] and [25].

7 Parameter Identification - Stage 2 and model validation

Different dynamic models were used to estimate the initial guess of parameters in stage 1 as discussed in section 4. The parameters identified in stage 1 were used as an initial guess for stage 2 optimization, which involved optimization using the plant and control oriented models. Stage 2 optimization can also be considered to be model validation, since it involved comparison of model outputs to experimental data.

A reference motor torque input measured experimentally (Fig. 22) to achieve a constant vehicle speed of 100 Km/hr was used as reference input to validate the plant and control-oriented models. A comparison of the plant outputs with the experimental data can be seen in Fig. 23. A good co-relation can be seen in the wheel torque, wheel and vehicle speeds. Small differences between experiments and models can be attributed to the following:

(a) Differences in effective tire radius. The effective tire radius in the plant model is calculated by the custom tire component based on dynamic changes in load as discussed in section 5 while the control-oriented model assumes a constant tire radius.

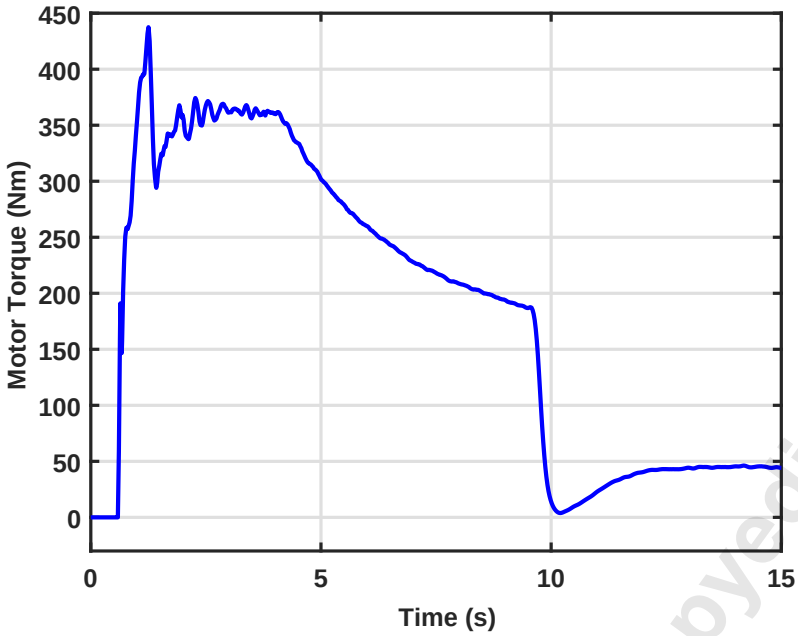

Fig. 22: Motor torque input measured experimentally

(b) Small differences in parameters (B, C, D and E) identified for the Pacejka tire model (4) and the relaxation length model (35).

A list of all the parameters identified for the plant and control-oriented models is given in Table 2 and 3 respectively.

8 Conclusion

The paper demonstrates a quick and accurate method for identifying parameters of a longitudinal dynamics model of an EV based on road testing. A real-time implementable, 18 DOF longitudinal dynamics plant model is presented. Two different control-oriented models for anti-jerk control of electric vehicles have been discussed. The control-model which aims at controlling wheel slip in addition to halfshaft torque is of particular interest, since slipping of wheel often occurs in EVs due to sudden changes in torque, especially during tip-in and tip-out maneuvers. The models have been validated against experimental data collected from the vehicle. Future work will involve design of a MPC based anti-jerk traction and cruise controller, based on the slip-based model, to reduce jerk and damp driveline oscillations.

Acknowledgements

We would like to thank Toyota, Automotive Partnerships Canada and the Natural Sciences and Engineering Research Council of Canada (NSERC) as sponsors of this research. A special thanks to our research engineer, Chris Shum, who enabled synchronous recording of signals from the Vehicle Measurement System (by AnD Technologies) and IMU using the CAN integration device.

Journal of Computational and Nonlinear Dynamics. Received December 06, 2017;
Accepted manuscript posted July 16, 2018. doi:10.1115/1.4040870

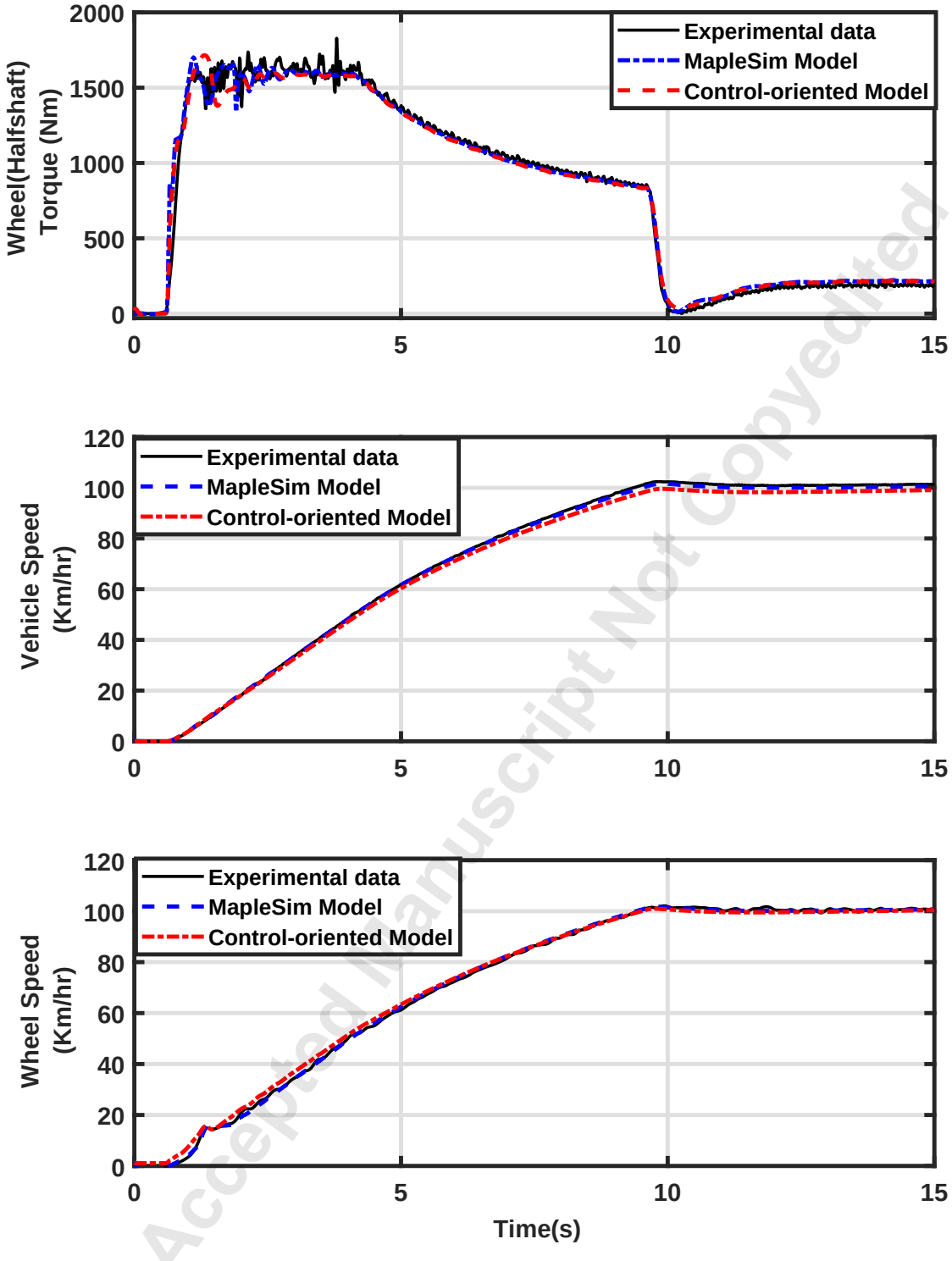

Fig. 23: Comparison of wheel torque, vehicle speeds and wheel speeds - plant, control-oriented model and experimental data

Appendix A: Parameters for Longitudinal Dynamics Model

Parameter	Symbol	Stage 1	Stage 2	Units
Weight of car	M	1850	1750	kg
Wheel base	L	2.66	2.66	m
Frontal area	A_f	2.46	2.79	m^2
Parameters for longitudinal force				
Pacejka Tire Model	B, C, D, E	49,1.37, 1.25,0.01	49,1.37, 1.25,0.01	–
Suspension stiffness	K_f, K_r	54,370, 35,540	54,370, 35,540	N/m
Suspension damping	C_f, C_r	1980,1795	1980,1795	Ns/m
Pitch inertia of car	I_y	3052	3052	kgm^2
Position of CG	l_r, h	1.15, 0.62	1.15, 0.62	m
Parameters for Aerodynamic drag and Rolling resistance				
Coeff of drag	C_d	0.308	0.382	–
Coeff of roll resistance	f_{rr}	0.0015	0.0015	–
Inertial parameters				
Drivetrain inertia	J_d	0.25	0.423	kgm^2
Wheel inertia	J_w	2.72	7.8	kgm^2
Height of center of pressure	h_d	0.689	0.689	m
Long. CG from rear wheel	l_r	1.42	1.15	m
Halfshaft stiffness	k	22,555	21,600	Nm/rad
Halfshaft damping	c	200	1494	Nm/rad/s

Table 2: Parameters of plant and motor model: Rav4EV

Appendix B: Parameters for Control-Oriented Model

Parameter	Symbol	Value	Units
Weight of car	M	1750	kg
Wheel base	L	2.66	m
Frontal area	A_f	2.79	m^2
Parameters for longitudinal force			
Pacejka Tire Model	B,C,D,E	49.04,1.02,1.10,0.001	–
Position of CG	l_r, h	1.48, 0.526	m
Normal force on tire	F_z	5500	N
Dynamic radius of tire	r_{eff}	0.357	m
Parameters for Aerodynamic drag and Rolling resistance			
Coeff of drag	C_d	0.7	–
Coeff of roll resistance	f_{rr}	0.002	–
Inertial parameters			
Drivetrain inertia	J_d	0.25	kgm^2
Wheel inertia	J_w	4	kgm^2
Long. CG from rear wheel	l_r	1.48	m
Halfshaft stiffness	k	21,600	Nm/rad
Halfshaft damping	c	1000	Nm/rad/s

Table 3: Parameters of control-oriented model: Rav4EV

References

[1] Gobbi, M., Mastinu, G., and Previati, G., 2011. "A method for measuring the inertia properties of rigid bodies". *Mechanical Systems and Signal Processing,* **25**(1), pp. 305–318.

[2] Shapiro, S. C., Dickerson, C. P., Arndt, S. M., Arndt, M. W., and Mowry, G. A., 1995. Error analysis of center-of-gravity measurement techniques. Tech. rep., SAE Technical Paper.

[3] Vehicle Test Facilities - IKA, RWTH. https://www.ika.rwth-aachen.de/images/forschung/pruefstaende/pruefstandskatalog-en.pdf. [Accessed on 15 Nov 2017].

[4] Bhoopalam, A. K., and Kefauver, K., 2015. Using surface texture parameters to relate flat belt laboratory traction data to the road. Tech. rep., SAE Technical Paper.

[5] Lo Conte, D., 2010. "Tyre parameter identification from road tests on a complete vehicle". Master's thesis, Delft University of Technology, Netherlands.

[6] Wilhelm, E., Bornatico, R., Widmer, R., Rodgers, L., and Soh, G. S., 2012. "Electric vehicle parameter identification". In EVS26 International Battery, Hybrid and Fuel Cell Electric Vehicle Symposium, Los Angeles, California, pp. 1–10.

[7] Amann, N., Bocker, J., and Prenner, F., 2004. "Active damping of drive train oscillations for an electrically driven vehicle". *IEEE/ASME Transactions on Mechatronics,* **9**(4), pp. 697–700.

[8] Lagerberg, A., and Egardt, B., 2005. "Model predictive control of automotive powertrains with backlash". *IFAC Proceedings Volumes,* **38**(1), pp. 1–6.

[9] Kawamura, H., Ito, K., Karikomi, T., and Kume, T., 2011. Highly-responsive acceleration control for the nissan leaf electric vehicle. Tech. rep., SAE Technical Paper.

[10] , 2015. Simulink design optimization guide. Matlab documentation (Version 2.8), Sep. http://www.mathworks.com/help/sldo/parameter-estimation.html.

[11] Pacejka, H. B., and Bakker, E., 1992. "The magic formula tyre model". *Vehicle System Dynamics,* **21**(S1), pp. 1–18.

[12] Emam, M. A., 2011. "A new empirical formula for calculating vehicles' frontal area". *SAE Technical Paper*(2011-01-0763).

[13] White, R. A., and Korst, H. H., 1972. "The determination of vehicle drag contributions from coast-down tests". *SAE Technical Paper*(720099).

[14] Yi, K., Hedrick, K., and Lee, S.-C., 1999. "Estimation of tire-road friction using observer based identifiers". *Vehicle System Dynamics,* **31**(4), pp. 233–261.

[15] Schmitke, C., Morency, K., and McPhee, J., 2008. "Using graph theory and symbolic computing to generate efficient models for multi-body vehicle dynamics". *Proceedings of the Institution of Mechanical Engineers, Part K: Journal of Multi-body Dynamics,* **222**(4), pp. 339–352.

[16] Eriksson, L., and Nielsen, L., 2014. *Modeling and control of engines and drivelines*. John Wiley & Sons.

[17] De Wit, C. C., and Tsiotras, P., 1999. "Dynamic tire friction models for vehicle traction control". In Decision and Control, 1999. Proceedings of the 38th IEEE Conference on, Vol. 4, IEEE, pp. 3746–3751.

[18] Reimpell, J., Burckhardt, M., Preukschat, A., and Zomotor, A., 1993. *Fahrwerktechnik: Radschlupf-Regelsysteme: Reifenverhalten, Zeitabläufe, Messung des Drehzustands der Räder, Anti-Blockier-System (ABS)-Theorie, Hydraulikkreisläufe, Antriebs-Schlupf-Regelung (ASR)-Theorie, Hydraulikkreisläufe, elektronische Regeleinheiten, Leistungsgrenzen, ausgeführte Anti-Blockier-Systeme und Antriebs-Schlupf-Regelungen*. Vogel.

[19] Kiencke, U., and Daiss, A., 1995. "Estimation of tyre friction for enhanced abs-systems". *Jsae Review,* **2**(16), p. 221.

[20] Pacejka, H. B., and Sharp, R. S., 1991. "Shear force development by pneumatic tyres in steady state conditions: a review of modelling aspects". *Vehicle system dynamics,* **20**(3-4), pp. 121–175.

[21] Maurice, J., and Pacejka, H., 1997. "Relaxation length behaviour of tyres". *Vehicle System Dynamics,* **27**(S1), pp. 339–342.

[22] Vantsevich, V. V., and Gray, J. P., 2015. "Relaxation length review and time constant analysis for agile tire dynamics control". In ASME 2015 International Design Engineering Technical Conferences and Computers and Information in Engineering Conference, no. DETC 2015-46798, American Society of Mechanical Engineers.

[23] Clover, C., and Bernard, J., 1998. "Longitudinal tire dynamics". *Vehicle System Dynamics,* **29**(4), pp. 231–260.

[24] Batra, M., McPhee, J., and Azad, N. L., Dec 2017. "Anti-jerk model predictive cruise control for connected EVs with

changing road conditions". In 2017 Asian Control Conference, 17 - 20 December 2017, Gold Coast, Australia.

[25] Batra, M., McPhee, J., and Azad, N. L., May 2018. "Non-linear model predictive anti-jerk cruise control for electric vehicles with slip-based constraints". In American Control Conference, American Control Conference, IEEE, June 27-29, 2018, Wisconsin Center, Milwaukee, USA.